

THE ENVIRONMENTAL DEPENDENCE OF LOW- z LY α ABSORPTION

DAVID M. FRENCH, BART P. WAKKER¹

¹*Department of Astronomy, University of Wisconsin, Madison, WI 53706, USA*

ABSTRACT

We present the results of a large-scale study of the Ly α -probed CGM of nearby galaxies. We have identified 1135 Ly α absorbers in the spectra of 264 background QSOs in the redshift range $0 \leq z \leq 0.033$, and correlated their positions with the surrounding galaxy environment. This has produced a sample of XXXX Ly α component-galaxy pairs, representing the largest-to-date dataset of this kind. By employing the likelihood-based matching scheme of French & Wakker (2017), we quantify the absorber-galaxy spacial correlation and identify 4 distinct absorber sub-samples based on their relative isolation from surrounding galaxies. We find that absorber equivalent width and Doppler-b parameter are enhanced with increasing proximity to galaxies.

Keywords: galaxies: intergalactic medium, galaxies: evolution, galaxies: halos, quasars: absorption lines

1. INTRODUCTION

The relationship between high column-density H I absorption ($N(\text{H I}) \gtrsim 10^{14} \text{ cm}^{-2}$) and galaxies has been well studied in the past several decades (e.g., Lanzetta et al. 1995; Bowen et al. 1998, 2002; Chen et al. 2003; Chen & Tinker 2008; Steidel et al. 2010; ?). **What do these studies find?** Relatively few studies have probed the Ly α -forest - galaxy relationship below this column density however (e.g., Wakker & Savage 2009; French & Wakker 2017; Bowen et al. 2002). The most obvious reason for this is due to the technically demanding nature of detecting these weak absorption systems. The installation of the Cosmic Origins Spectrograph (COS) on the Hubble Space Telescope (*HST*) in ??2011?? however has finally opened a window to study this rich reservoir of intergalactic gas. Thanks to the high throughput and sensitivity available with COS, a large number of distant quasi-stellar objects (QSOs) have been observed with sufficiently high signal-to-noise for a large variety of science priorities.

...

The second major challenge for galaxy-absorber correlation studies is obtaining data on the galaxies. While the resolution of absorption line spectroscopy is redshift-independent (e.g., a $N(\text{H I}) \gtrsim 10^{13} \text{ cm}^{-2}$ Ly α absorber is just as readily detected at $z \sim 0$ as at $z \sim 1$), detecting and classifying galaxies is a photometric exercise whose difficulty rapidly increases with redshift. Thus, while we wish to include all absorption systems in any particular sightline observation to maximize our sample size, we are instead limited by our ability to produce a matching galaxy sample. Different studies have gone about tackling this issue in different ways. ...

To make progress here we have completed the largest-to-date survey of low- $N(\text{H I})$ Ly α absorbers in the lo-

cal Universe and their relationship to nearby galaxies. This survey is made possible by taking advantage of the large archival sample of COS QSO sightlines, and the high completeness of existing galaxy data in the redshift range $cz \leq 10,000 \text{ km s}^{-1}$. In Section 2 we present the datasets, sample selection, and galaxy-absorber matching methods. In Section 3 we present and discuss the results of the galaxy-absorber correlation, and in Section 4 we offer our conclusions and discuss areas of future work.

2. DATA ANALYSIS

In this section we discuss the selection and reduction of our sample of archival QSO spectra taken by the Cosmic Origins Spectrograph (COS) on *HST*. There currently exist over 700 COS spectra in the Barbara A. Mikulski Archive for Space Telescopes (MAST) with G130M exposures which cover the Ly α transition in our survey's redshift range ($cz \leq 10,000 \text{ km s}^{-1}$). In order to choose the most useful spectra for our purposes, we first sort them by signal-to-noise (SN) and make a cut at approximately SN=10. A signal-to-noise of approximately 10 or higher measured near 1238Å allows us to detect an absorption feature down to an equivalent width of $\sim 50 \text{ m}\text{\AA}$ at 5σ . We then correlate the resulting (SN $\gtrsim 10$) sample with our galaxy catalog (see ??), and sort the spectra by proximity to a galaxy. While this introduces a slight bias against void or isolated absorption features, we are presently most interested in the absorber-galaxy relation and therefore choose this method to maximize the associated absorber-galaxy sample size. Additionally, because this sorting is done without knowledge of line locations, we will end up with significant sample of isolated absorbers simply based on their velocity, or z -direction, isolation from galaxies. Finally, from this galaxy-proximity sorted spectra list we

Note also that many of the sightlines were not observed because of their proximity to a nearby galaxy. Most were observed to study systems at $z > 0.03$, so in terms of the galaxies at $z < 0.03$ the sample is mostly a random set of sightlines.

choose 264 targets based on the relative ease of spectral feature identification.

Data reduction, continuum fitting and line measurement are then conducted in an identical fashion to French & Wakker (2017). In short, we determine the continuum around each line by fitting a 1st, 2nd or 3rd order polynomial to the line-free regions around each feature. All equivalent width measurements are integrated based on this fit, and we calculate the second moment of the apparent optical depth profiles to determine Doppler b -parameters. Table 1 summarizes the QSO targets included in this work.

In this sample of 264 QSOs we have detected 1135 Ly α absorbers. Figures 1 and 2 show all-sky maps of the positions of all absorbers split into 4 velocity bins ($v_{\text{Ly}\alpha} = [0 - 2500]$, $(2500 - 5000]$, $(5000 - 7500]$, and

$(7500 - 10,000] \text{ km s}^{-1}$). The distribution of galaxies in the same velocity ranges are include here also (galaxies are plotted as small circles, absorbers as stars; see Chapter 1). Comparing the galaxy to absorber positions and velocities within each velocity range by eye, we can clearly see that the Ly α absorbers broadly trace the locations of the galaxies. If the current Lambda Cold Dark Matter (Λ CDM) cosmology is to be believed, this should not be remarkably surprising. The baryons from which galaxies are built and those found within the IGM and traced by Ly α absorption should both follow the underlying potential produced by the Dark Matter, and should therefore be found in similar places. Beyond this big-picture result however, we want to know how the absorbers react to the presence of the galaxies on a more local scale.

Table 1. Summary of QSO Sample

Target (1)	R.A. (2)	Dec. (3)	z (4)	Program (5)	T_{exp} (ks) (6)
PHL2525	0.0 0.0 24.4	-12.0 45.0 48.0	0.2	12604	2146
PG0003+158	0.0 5.0 59.2	16.0 9.0 49.0	0.4509	12038	10361
MRK335	0.0 6.0 19.5	20.0 12.0 11.0	0.02578	11524	5122
4C25.01	0.0 19.0 39.8	26.0 2.0 52.0	0.284	14268	3739
UM228	0.0 21.0 1.0	0.0 52.0 47.0	0.0983	13017	1060
RX_J0023.5+1547	0.0 23.0 30.6	15.0 47.0 45.0	0.41188	14071	7431
RX_J0028.1+3103	0.0 28.0 10.7	31.0 3.0 48.0	0.5	14268	3714
PG0026+129	0.0 29.0 13.7	13.0 16.0 4.0	0.142	12569	1868
Zw535.012	0.0 36.0 21.0	45.0 39.0 54.0	0.04764	14268	5234
ESO350-IG38	0.0 36.0 52.9	-33.0 33.0 19.0	0.0206	13017	1536
RX_J0043.6+3725	0.0 43.0 42.5	37.0 25.0 20.0	0.0799	14268	5532
RX_J0048.3+3941	0.0 48.0 19.0	39.0 41.0 12.0	0.134	11632	13484
RX_J0050.8+3536	0.0 50.0 50.7	35.0 36.0 43.0	0.058	14268	3679
MRK1502	0.0 53.0 34.9	12.0 41.0 36.0	0.06114	12569	9488
RX_J0053.7+2232	0.0 53.0 46.1	22.0 32.0 23.0	0.148	14268	3749
PG0052+251	0.0 54.0 52.1	25.0 25.0 39.0	0.155	14268	2497
TON_S180	0.0 57.0 20.0	-22.0 22.0 56.0	0.06198	8109	1260
HE0056-3622	0.0 58.0 37.4	-36.0 6.0 5.0	0.16414	12604	4959
MS0117.2-2837	1.0 19.0 35.7	-28.0 21.0 32.0	0.347	12204	5233
TON_S210	1.0 21.0 51.5	-28.0 20.0 58.0	0.116	12204	5047
FAIRALL9	1.0 23.0 45.8	-58.0 48.0 21.0	0.04702	12604	4960
SDSSJ014143.20+134032.0	1.0 41.0 43.2	13.0 40.0 32.0	0.04541	12275	7669
FBS0150+396	1.0 53.0 6.7	39.0 55.0 45.0	0.2119	14268	5022
PHL1226	1.0 54.0 28.0	4.0 48.0 18.0	0.404	12536	14542
HE0153-4520	1.0 55.0 13.2	-45.0 6.0 11.0	0.451	11541	5228
SDSSJ015530.02-085704.0	1.0 55.0 30.0	-8.0 57.0 4.0	0.16443	12248	2931
RXS_J0155.6+3115	1.0 55.0 36.0	31.0 15.0 18.0	0.135	14268	11948
MRK1014	1.0 59.0 50.2	0.0 23.0 41.0	0.16308	12569	1828
SDSSJ015952.95+134554.3	1.0 59.0 53.0	13.0 45.0 54.0	0.50378	12603	7623
3C57	2.0 1.0 57.2	-11.0 32.0 33.0	0.669	12038	10963
SDSSJ021218.32-073719.8	2.0 12.0 18.3	-7.0 37.0 20.0	0.17392	12248	6525
3C66A	2.0 22.0 39.6	43.0 2.0 8.0	0.444	12612	12600

Table 1 continued

align better gives z to same accuracy in all cases.

It is probably more efficient to combine this table with the table with detections.

At least need the S/N near 1238 A for each of these sightlines here.

Table 1 (*continued*)

Target	R.A.	Dec.	z	Program	T_{exp}
(1)	(2)	(3)	(4)	(5)	(ks) (6)
HE0226-4110	2.0 28.0 15.2	-40.0 57.0 15.0	0.495	11541	6775
MRK1179	2.0 33.0 22.4	27.0 56.0 13.0	0.0376	14268	5573
NGC985	2.0 34.0 37.8	-8.0 47.0 17.0	0.04354	12953	7111
HE0241-3043	2.0 43.0 37.7	-30.0 30.0 48.0	0.66929	12988	6972
2dFGRS_S393Z082	2.0 45.0 0.8	-30.0 7.0 23.0	0.33921	12988	17668
MS0244.6-3020	2.0 46.0 49.9	-30.0 7.0 42.0	0.53	12988	12230
HE0340-2703	3.0 42.0 20.5	-26.0 53.0 59.0	0.283	9378	4895
PKS0405-12	4.0 7.0 48.4	-12.0 11.0 37.0	0.57259	11508	24147
1H0419-577	4.0 26.0 0.7	-57.0 12.0 2.0	0.104	11686	20429
HE0429-5343	4.0 30.0 40.0	-53.0 36.0 56.0	0.04001	12275	2067
HE0435-5304	4.0 36.0 50.9	-52.0 58.0 47.0	0.42616	11520	8372
RBS563	4.0 38.0 29.2	-61.0 47.0 59.0	0.069	11692	4628
RBS567	4.0 39.0 38.7	-53.0 11.0 31.0	0.243	11520	8176
HE0439-5254	4.0 40.0 12.0	-52.0 48.0 18.0	1.053	11520	8402
PKS0558-504	5.0 59.0 47.4	-50.0 26.0 52.0	0.137	11692	1075
IRAS_Z06229-6434	6.0 23.0 7.6	-64.0 36.0 21.0	0.12889	11692	8728
RX_J0714.5+7408	7.0 14.0 36.2	74.0 8.0 10.0	0.371	12275	8333
MRK380	7.0 19.0 50.8	74.0 27.0 57.0	0.475	12275	5491
1H0717+714	7.0 21.0 53.5	71.0 20.0 36.0	0.23149	12025	6000
FBQSJ0751+2919	7.0 51.0 12.3	29.0 19.0 38.0	0.91573	11741	16531
SDSSJ080838.80+051440.0	8.0 8.0 38.8	5.0 14.0 40.0	0.36061	12603	4674
SDSSJ080908.13+461925.6	8.0 9.0 8.1	46.0 19.0 26.0	0.65873	12248	3146
PG0804+761	8.0 10.0 58.7	76.0 2.0 43.0	0.102	11686	5510
SDSSJ082024.20+233450.0	8.0 20.0 24.2	23.0 34.0 50.0	0.47056	11598	5035
PG0832+251	8.0 35.0 35.8	24.0 59.0 40.0	0.331	12025	6134
SDSSJ084159.20+140642.0	8.0 41.0 59.1	14.0 6.0 42.0	1.252	13314	11204
PG0838+770	8.0 44.0 45.3	76.0 53.0 9.0	0.131	11520	8865
PG0844+349	8.0 47.0 42.5	34.0 45.0 5.0	0.064	12569	1900
FBQSJ0908+3246	9.0 8.0 38.8	32.0 46.0 20.0	0.25989	14240	7430
TON1009	9.0 9.0 6.2	32.0 36.0 30.0	0.81028	12603	4740
TON1015	9.0 10.0 37.0	33.0 29.0 24.0	0.354	14240	4774
SDSSJ091052.80+333008.0	9.0 10.0 52.8	33.0 30.0 8.0	0.11631	14240	7442
SDSSJ091127.30+325337.0	9.0 11.0 27.3	32.0 53.0 37.0	0.29038	14240	10028
SDSSJ091728.60+271951.0	9.0 17.0 28.6	27.0 19.0 51.0	0.07564	14071	15471
MRK106	9.0 19.0 55.3	55.0 21.0 37.0	0.12337	12029	6538
PG0923+201	9.0 25.0 54.7	19.0 54.0 5.0	0.19	12569	1860
RX_J0925.9+4535	9.0 25.0 54.4	45.0 35.0 44.0	0.329	12248	4436
US645	9.0 29.0 9.8	46.0 44.0 24.0	0.24	12248	2415
SDSSJ093706.90+170021.0	9.0 37.0 6.9	17.0 0.0 21.0	0.50567	12603	7635
HS0943+4725	9.0 46.0 21.3	47.0 11.0 31.0	0.23	12248	4436
SDSSJ094840.10+580038.0	9.0 48.0 40.1	58.0 0.0 39.0	0.49179	13774	8835
IRAS_F09539-0439	9.0 56.0 30.2	-4.0 53.0 16.0	0.157	12275	7696
PG0953+414	9.0 56.0 52.4	41.0 15.0 22.0	0.2341	12038	4785
3C232	9.0 58.0 20.9	32.0 24.0 2.0	0.5306	5892	54208
SDSSJ095914.80+320357.0	9.0 59.0 14.8	32.0 3.0 57.0	0.56462	12603	2273
SDSSJ095915.60+050355.0	9.0 59.0 15.7	5.0 3.0 55.0	0.16263	12248	2931
SBS0957+599	10.0 1.0 2.6	59.0 44.0 14.0	0.74749	12248	3300
PG1001+291	10.0 4.0 2.6	28.0 55.0 35.0	0.3272	12038	6199
PG1001+054	10.0 4.0 20.1	5.0 13.0 0.0	0.161	13347	5233
PG1004+130	10.0 7.0 26.1	12.0 48.0 56.0	0.24	12569	4107
TON488	10.0 10.0 0.7	30.0 3.0 22.0	0.25643	12025	10796
TON1187	10.0 13.0 3.1	35.0 51.0 22.0	0.07	12275	1958

Table 1 continued

Table 1 (*continued*)

Target	R.A.	Dec.	z	Program	T_{exp}
(1)	(2)	(3)	(4)	(5)	(ks) (6)
PG1011-040	10.0 14.0 20.7	-4.0 18.0 41.0	0.058	11524	5365
UVQ SJ101629.20-315023.6	10.0 16.0 29.2	-31.0 50.0 24.0	0.2417	14687	5044
RX_J1017.5+4702	10.0 17.0 31.0	47.0 2.0 25.0	0.33544	13314	8655
RBS877	10.0 31.0 18.5	50.0 53.0 36.0	0.3604	12025	14651
HE1029-1401	10.0 31.0 54.4	-14.0 16.0 52.0	0.086	7345	7535
SDSS J104241.30+250123.0	10.0 42.0 41.3	25.0 1.0 23.0	0.343	14071	10068
SDSS J104335.90+115129.0	10.0 43.0 35.9	11.0 51.0 29.0	0.794	14071	4736
VII Zw348	10.0 51.0 0.7	65.0 59.0 40.0	0.03251	13654	4241
PG1048+342	10.0 51.0 43.9	33.0 59.0 27.0	0.167	12024	7814
CSO295	10.0 52.0 5.6	36.0 40.0 40.0	0.609	14772	1088
RX_J1054.2+3511	10.0 54.0 16.2	35.0 11.0 24.0	0.203	14772	533
RBS918	10.0 54.0 44.7	48.0 31.0 39.0	0.286	14772	566
MRK1269	10.0 55.0 19.5	40.0 27.0 17.0	0.12	14772	1189
SDSS J105945.30+144142.0	10.0 59.0 45.2	14.0 41.0 43.0	0.63171	12248	4217
RX_J1100.8+2839	11.0 0.0 52.3	28.0 38.0 1.0	0.243	13749	4659
H1101-232	11.0 3.0 37.7	-23.0 29.0 31.0	0.186	12025	13341
TON52	11.0 4.0 6.9	31.0 41.0 11.0	0.43572	12248	2982
3C249.1	11.0 4.0 14.0	76.0 58.0 58.0	0.3115	4939	19157
MRK421	11.0 4.0 27.3	38.0 12.0 32.0	0.03002	11520	3684
HS1102+3441	11.0 5.0 39.8	34.0 25.0 35.0	0.51	11541	11381
SBS1108+560	11.0 11.0 32.2	55.0 47.0 26.0	0.76827	12025	8387
HS1111+4309	11.0 13.0 57.4	42.0 53.0 26.0	0.442	14772	1199
SDSS J111443.70+525834.0	11.0 14.0 43.7	52.0 58.0 34.0	0.07921	14240	13440
PG1112+431	11.0 15.0 6.0	42.0 49.0 49.0	0.30064	12275	7942
RX_J1117.6+5301	11.0 17.0 40.5	53.0 1.0 51.0	0.15871	14240	4943
PG1115+407	11.0 18.0 30.3	40.0 25.0 54.0	0.154	11519	5109
PG1116+215	11.0 19.0 8.7	21.0 19.0 18.0	0.1765	12038	4677
SDSS J111908.70+254505.0	11.0 19.0 8.7	25.0 45.0 5.0	0.58	14772	2352
SBS1116+523	11.0 19.0 47.9	52.0 5.0 53.0	0.35568	14240	4949
SDSS J112005.00+041323.0	11.0 20.0 5.0	4.0 13.0 23.0	0.54689	12603	4708
CSO1161	11.0 20.0 7.4	42.0 35.0 51.0	0.227	14772	1715
ESO265-G23	11.0 20.0 48.0	-43.0 15.0 50.0	0.056	12275	1983
RBS970	11.0 20.0 48.1	42.0 12.0 13.0	0.124	14772	1735
RX_J1121.2+0326	11.0 21.0 14.0	3.0 25.0 47.0	0.152	12248	2695
SDSS J112224.10+031802.0	11.0 22.0 24.1	3.0 18.0 2.0	0.47528	12603	7588
SDSS J112439.50+113117.0	11.0 24.0 39.4	11.0 31.0 17.0	0.143	14071	10427
PG1121+423	11.0 24.0 39.2	42.0 1.0 45.0	0.225	12024	5035
SDSS J112448.30+531818.0	11.0 24.0 48.3	53.0 18.0 19.0	0.53151	14240	7920
RX_J1125.0+2513	11.0 25.0 3.7	25.0 13.0 2.0	0.271	14772	1068
RBS982	11.0 25.0 40.8	41.0 22.0 32.0	0.196	14772	1197
SBS1122+594	11.0 25.0 53.8	59.0 10.0 22.0	0.85142	11520	9874
MRK1298	11.0 29.0 16.7	-4.0 24.0 7.0	0.06	12569	15595
MRK1447	11.0 30.0 29.1	49.0 34.0 58.0	0.096	14772	2478
TON580	11.0 31.0 9.5	31.0 14.0 5.0	0.289	11519	4903
FBQS J1134+2555	11.0 34.0 57.6	25.0 55.0 28.0	0.70994	12248	4235
HE1136-1334	11.0 39.0 10.7	-13.0 50.0 43.0	0.55646	12275	7669
3C263	11.0 39.0 57.0	65.0 47.0 49.0	0.646	11541	15360
RX_J1140.1+4115	11.0 40.0 3.4	41.0 15.0 4.0	0.072	14772	1751
SDSS J114046.10+113649.0	11.0 40.0 46.1	11.0 36.0 50.0	0.687	14071	10129
CSO1208	11.0 40.0 47.9	46.0 22.0 5.0	0.115	14729	3052
US2816	11.0 42.0 12.3	30.0 16.0 13.0	0.4819	12603	4790
RX_J1142.5+2503	11.0 42.0 31.8	25.0 3.0 38.0	0.185	14772	1822

Table 1 continued

Table 1 (*continued*)

Target	R.A.	Dec.	z	Program	T_{exp}
(1)	(2)	(3)	(4)	(5)	(ks) (6)
RX_J1142.7+4625	11.0 42.0 41.2	46.0 24.0 36.0	0.115	14772	2368
RBS1024	11.0 44.0 29.9	36.0 53.0 9.0	0.04	14772	1183
SDSSJ114646.00+371511.0	11.0 46.0 46.0	37.0 15.0 12.0	0.295	14772	1082
PG1148+549	11.0 51.0 20.5	54.0 37.0 33.0	0.969	11741	17823
CSO1245	11.0 56.0 30.1	42.0 52.0 55.0	1.014	14772	1205
SDSSJ115722.40+114040.0	11.0 57.0 22.4	11.0 40.0 41.0	0.291	14071	10034
HE1159-1338	12.0 1.0 58.7	-13.0 55.0 0.0	0.506	12275	7669
RX_J1210.7+2725	12.0 10.0 45.6	27.0 25.0 36.0	0.231	14772	1802
CSO395	12.0 11.0 14.6	36.0 57.0 40.0	0.17109	12248	3012
RX_J1212.2+2803	12.0 12.0 17.2	28.0 3.0 50.0	0.167	14772	1814
PG1211+143	12.0 14.0 17.7	14.0 3.0 13.0	0.0809	13947	2320
SDSSJ121640.60+071224.0	12.0 16.0 40.6	7.0 12.0 24.0	0.58756	11698	2048
RX_J1217.2+2749	12.0 17.0 15.3	27.0 49.0 51.0	0.3941	14772	2312
RBS1090	12.0 17.0 21.4	30.0 56.0 31.0	0.307	14772	2318
TON605	12.0 17.0 52.1	30.0 7.0 1.0	0.13	13651	7369
PG1216+069	12.0 19.0 20.9	6.0 38.0 38.0	0.3313	12025	5146
MS1217.0+0700	12.0 19.0 30.9	6.0 43.0 35.0	0.08058	13444	4639
HE1217+0220	12.0 20.0 11.9	2.0 3.0 42.0	0.24	13852	2052
LBQS1218+1611	12.0 21.0 2.5	15.0 54.0 47.0	0.22945	11698	2263
PG1218+304	12.0 21.0 21.9	30.0 10.0 37.0	0.182	14772	1818
WCom	12.0 21.0 31.7	28.0 13.0 58.0	0.102	14772	1071
MRK205	12.0 21.0 44.0	75.0 18.0 39.0	0.07085	4952	760
LBQS1220+1006	12.0 23.0 12.2	9.0 50.0 18.0	0.27692	11698	2258
3C273.0	12.0 29.0 6.7	2.0 3.0 9.0	0.15834	12038	4002
HE1228+0131	12.0 30.0 50.0	1.0 15.0 23.0	0.117	11686	11036
MS1228.6+1219	12.0 31.0 13.1	12.0 3.0 7.0	0.11612	14071	10419
MRK771	12.0 32.0 3.6	20.0 9.0 30.0	0.06301	12569	1868
LBQS1230-0015	12.0 33.0 4.1	-0.0 31.0 34.0	0.47095	11598	10323
HS1231+4814	12.0 33.0 35.1	47.0 58.0 1.0	0.38223	11598	5929
RX_J1236.0+2641	12.0 36.0 4.0	26.0 41.0 36.0	0.20915	12248	4235
SDSSJ124210.30+321427.0	12.0 42.0 10.3	32.0 14.0 27.0	1.49257	14085	13008
SDSSJ125846.70+242739.0	12.0 58.0 46.7	24.0 27.0 39.0	0.3711	13382	7546
US136	13.0 1.0 0.9	28.0 19.0 45.0	1.36	13314	13429
PG1259+593	13.0 1.0 12.9	59.0 2.0 7.0	0.4778	11541	9200
RX_J1303.7+2633	13.0 3.0 46.0	26.0 33.0 14.0	0.437	13382	7015
HS1302+2510	13.0 4.0 51.4	24.0 54.0 46.0	0.605	13382	5134
SDSSJ130524.30+035731.0	13.0 5.0 24.3	3.0 57.0 31.0	0.54566	12603	7588
PG1302-102	13.0 5.0 33.0	-10.0 33.0 20.0	0.2784	8306	22119
PG1307+085	13.0 9.0 47.0	8.0 19.0 48.0	0.155	12569	1836
PG1309+355	13.0 12.0 17.8	35.0 15.0 21.0	0.184	12569	1896
SDSSJ131545.20+152556.0	13.0 15.0 45.2	15.0 25.0 56.0	0.44811	12603	4688
RX_J1330.8+3119	13.0 30.0 53.3	31.0 19.0 31.0	0.24232	12248	4262
RX_J1342.1+0505	13.0 42.0 6.5	5.0 5.0 24.0	0.26608	12248	2931
RBS1307	13.0 42.0 31.3	38.0 29.0 4.0	0.1719	12248	3034
RX_J1342.7+1844	13.0 42.0 46.9	18.0 44.0 44.0	0.3832	12248	2938
HE1340-0038	13.0 42.0 51.6	-0.0 53.0 45.0	0.32654	11598	4606
PG1341+258	13.0 43.0 56.8	25.0 38.0 48.0	0.087	13314	8415
FBQSJ1353+3620	13.0 53.0 26.1	36.0 20.0 49.0	0.28504	13444	4777
SDSSJ135341.03+361948.0	13.0 53.0 41.0	36.0 19.0 48.0	0.14659	13444	10199
SDSSJ135424.90+243006.3	13.0 54.0 24.9	24.0 30.0 6.0	1.89283	12603	6829
PG1352+183	13.0 54.0 35.7	18.0 5.0 17.0	0.152	13448	4856
RX_J1356.4+2515	13.0 56.0 25.6	25.0 15.0 24.0	0.16404	12248	2282

Table 1 continued

Table 1 (*continued*)

Target	R.A.	Dec.	z	Program	T_{exp}
(1)	(2)	(3)	(4)	(5)	(ks) (6)
SDSSJ135712.60+170444.0	13.0 57.0 12.6	17.0 4.0 44.0	0.1505	12248	4223
SDSSJ135726.27+043541.4	13.0 57.0 26.3	4.0 35.0 41.0	1.23453	12264	14148
SDSSJ140428.30+335342.0	14.0 4.0 28.3	33.0 53.0 42.0	0.54996	12603	7705
SDSSJ141038.40+230447.0	14.0 10.0 38.4	23.0 4.0 47.0	0.7958	12958	11275
PG1411+442	14.0 13.0 48.3	44.0 0.0 14.0	0.0896	12569	14415
SDSSJ141542.90+163414.0	14.0 15.0 42.9	16.0 34.0 14.0	0.7435	12486	18479
SDSSJ141949.40+060654.0	14.0 19.0 49.4	6.0 6.0 54.0	1.64892	13473	11028
RX_J1426.2+1955	14.0 26.0 13.3	19.0 55.0 25.0	0.21	13314	5124
SDSSJ142859.10+322507.0	14.0 28.0 59.0	32.0 25.0 7.0	0.62717	13314	11314
RX_J1429.6+0321	14.0 29.0 40.7	3.0 21.0 26.0	0.25344	12603	3876
FBQ SJ1431+2442	14.0 31.0 25.8	24.0 42.0 20.0	0.40691	12603	16501
MRK817	14.0 36.0 22.0	58.0 47.0 40.0	0.03146	11505	3426
PG1435-067	14.0 38.0 16.2	-6.0 58.0 21.0	0.126	12569	1864
RX_J1500.5+5517	15.0 0.0 30.7	55.0 17.0 9.0	0.40481	12276	8422
RBS1454	15.0 2.0 4.1	6.0 45.0 16.0	0.286	12603	2239
RX_J1503.2+6810	15.0 3.0 16.4	68.0 10.0 6.0	0.114	12276	1932
QSO1500-4140	15.0 3.0 33.9	-41.0 52.0 24.0	0.335	8244	6000
MRK841	15.0 4.0 1.2	10.0 26.0 16.0	0.03642	13448	3060
SBS1503+570	15.0 4.0 55.6	56.0 49.0 20.0	0.35894	12276	5163
MRK1392	15.0 5.0 56.6	3.0 42.0 26.0	0.03613	13448	4846
SDSSJ150928.30+070235.0	15.0 9.0 28.3	7.0 2.0 35.0	0.41878	12603	7612
SDSSJ150952.20+111047.0	15.0 9.0 52.2	11.0 10.0 47.0	0.28494	12614	57130
SDSSJ151237.15+012846.0	15.0 12.0 37.2	1.0 28.0 46.0	0.26625	12603	7590
PG1522+101	15.0 24.0 24.5	9.0 58.0 29.0	1.32801	11741	16401
FBS1526+659	15.0 27.0 28.7	65.0 48.0 10.0	0.345	12276	2032
TON236	15.0 28.0 40.6	28.0 25.0 30.0	0.45	12038	6554
RBS1503	15.0 29.0 7.5	56.0 16.0 7.0	0.099	12276	1964
2E1530+1511	15.0 33.0 14.3	15.0 1.0 3.0	0.09	14071	9348
MRK290	15.0 35.0 52.3	57.0 54.0 9.0	0.02958	11524	3856
MRK486	15.0 36.0 38.4	54.0 33.0 33.0	0.03893	12276	5001
SBS1537+577	15.0 38.0 10.0	57.0 36.0 13.0	0.07342	12276	5193
HS1543+5921	15.0 44.0 20.3	59.0 12.0 27.0	0.807	8485	2139
RX_J1544.5+2827	15.0 44.0 30.5	28.0 27.0 56.0	0.23137	13423	2096
3C323.1	15.0 47.0 43.5	20.0 52.0 17.0	0.2643	13398	9841
PG1553+113	15.0 55.0 43.2	11.0 11.0 25.0	0.46699	11520	10840
SDSSJ160519.70+144852.2	16.0 5.0 19.7	14.0 48.0 52.0	0.3721	12614	8374
RX_J1608.3+6018	16.0 8.0 20.6	60.0 18.0 28.0	0.178	12276	5158
MRK876	16.0 13.0 57.2	65.0 43.0 11.0	0.129	9754	29200
NAB1612+26	16.0 14.0 10.6	26.0 32.0 50.0	0.395	14277	25413
1H1613-097	16.0 15.0 19.1	-9.0 36.0 13.0	0.06496	13448	4833
MRK877	16.0 20.0 11.3	17.0 24.0 28.0	0.11244	12569	1844
PG1626+554	16.0 27.0 56.1	55.0 22.0 32.0	0.133	12029	3318
KAZ447	17.0 3.0 29.0	61.0 41.0 10.0	0.07732	12276	5173
3C351.0	17.0 4.0 41.6	60.0 44.0 29.0	0.37194	8015	77012
H1821+643	18.0 21.0 57.2	64.0 20.0 36.0	0.297	11484	12039
RX_J1830.3+7312	18.0 30.0 23.2	73.0 13.0 11.0	0.123	8316	5842
HS1831+5338	18.0 32.0 49.7	53.0 40.0 22.0	0.039	12275	8284
ESO141-G55	19.0 21.0 14.3	-58.0 40.0 13.0	0.036	12936	2178
PKS2005-489	20.0 9.0 25.4	-48.0 49.0 54.0	0.071	11520	2461
RX_J2043.1+0324	20.0 43.0 6.3	3.0 24.0 52.0	0.271	13840	7834
MRK509	20.0 44.0 9.7	-10.0 43.0 24.0	0.0344	12022	14074
PG2112+059	21.0 14.0 52.6	6.0 7.0 42.0	0.466	13840	7891

Table 1 continued

Table 1 (*continued*)

Target	R.A.	Dec.	z	Program	T_{exp}
(1)	(2)	(3)	(4)	(5)	(ks) (6)
MRK1513	21.0 32.0 27.9	10.0 8.0 19.0	0.06298	11524	5513
IRAS_F21325-6237	21.0 36.0 23.1	-62.0 24.0 1.0	0.0588	12936	4230
RBS1768	21.0 38.0 49.9	-38.0 28.0 40.0	0.18299	12936	6962
RX_J2139.7+0246	21.0 39.0 44.2	2.0 46.0 6.0	0.26	13840	7854
RBS1795	21.0 54.0 51.1	-44.0 14.0 6.0	0.344	11541	8173
PKS2155-304	21.0 58.0 52.1	-30.0 13.0 32.0	0.116	5889	6682
MRK304	22.0 17.0 12.2	14.0 14.0 21.0	0.06576	12569	3950
RBS1892	22.0 45.0 20.3	-46.0 52.0 11.0	0.201	12604	2228
MRC2251-178	22.0 54.0 5.9	-17.0 34.0 55.0	0.06609	12029	5515
SDSSJ225738.20+134045.0	22.0 57.0 38.2	13.0 40.0 45.0	0.59455	11598	3428
HE2258-5524	23.0 1.0 52.0	-55.0 8.0 31.0	0.141	13444	5185
HE2259-5524	23.0 2.0 22.5	-55.0 8.0 27.0	0.8549	13444	10940
CTS487	23.0 22.0 11.0	-34.0 47.0 57.0	0.42	13448	8061
RBS2000	23.0 24.0 44.7	-40.0 40.0 49.0	0.17359	13448	5046
HE2332-3556	23.0 34.0 44.5	-35.0 39.0 47.0	0.11	13444	7378
RBS2023	23.0 34.0 52.5	-35.0 38.0 42.0	0.098	13444	10049
RBS2055	23.0 51.0 52.8	26.0 19.0 33.0	0.038	14268	7029
PG2349-014	23.0 51.0 56.1	-1.0 9.0 13.0	0.174	12569	1844
RBS2070	23.0 59.0 7.8	-30.0 37.0 39.0	0.16539	12864	17033

NOTE—Summary of COS targets in this study. **SORT THIS TABLE – EDIT R.A. AND DEC ALSO**

Galaxy colors scale is OK, but absorber absorption color scale is too hard to see.

Centering on 12h would be better

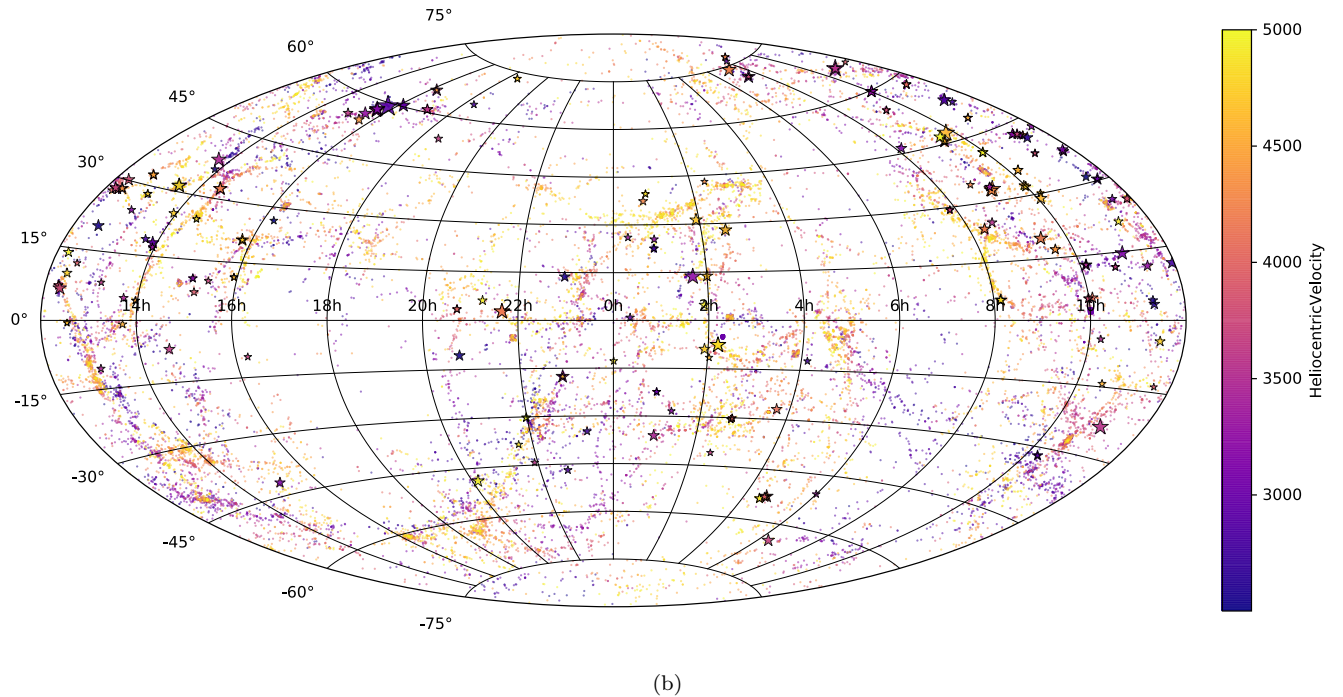
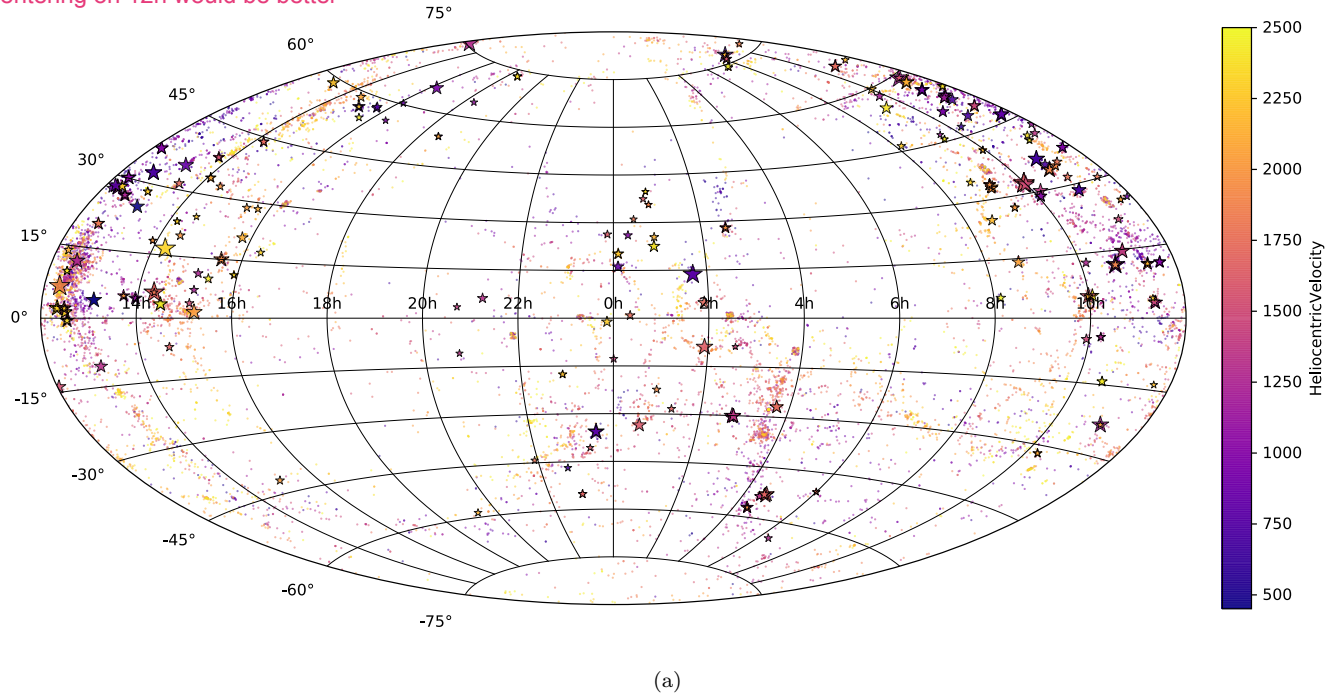


Figure 1. All sky maps of the locations of all absorbers and galaxies. Absorbers are plotted as stars and scaled in size based on their EW. Galaxies are plotted as dots. The colors of both galaxies and absorbers are mapped to their heliocentric velocities. (a) All galaxies and absorbers in the velocity range $450 \leq cz \leq 2500 \text{ km s}^{-1}$. (b) All galaxies and absorbers in the velocity range $2500 < cz \leq 5000 \text{ km s}^{-1}$.

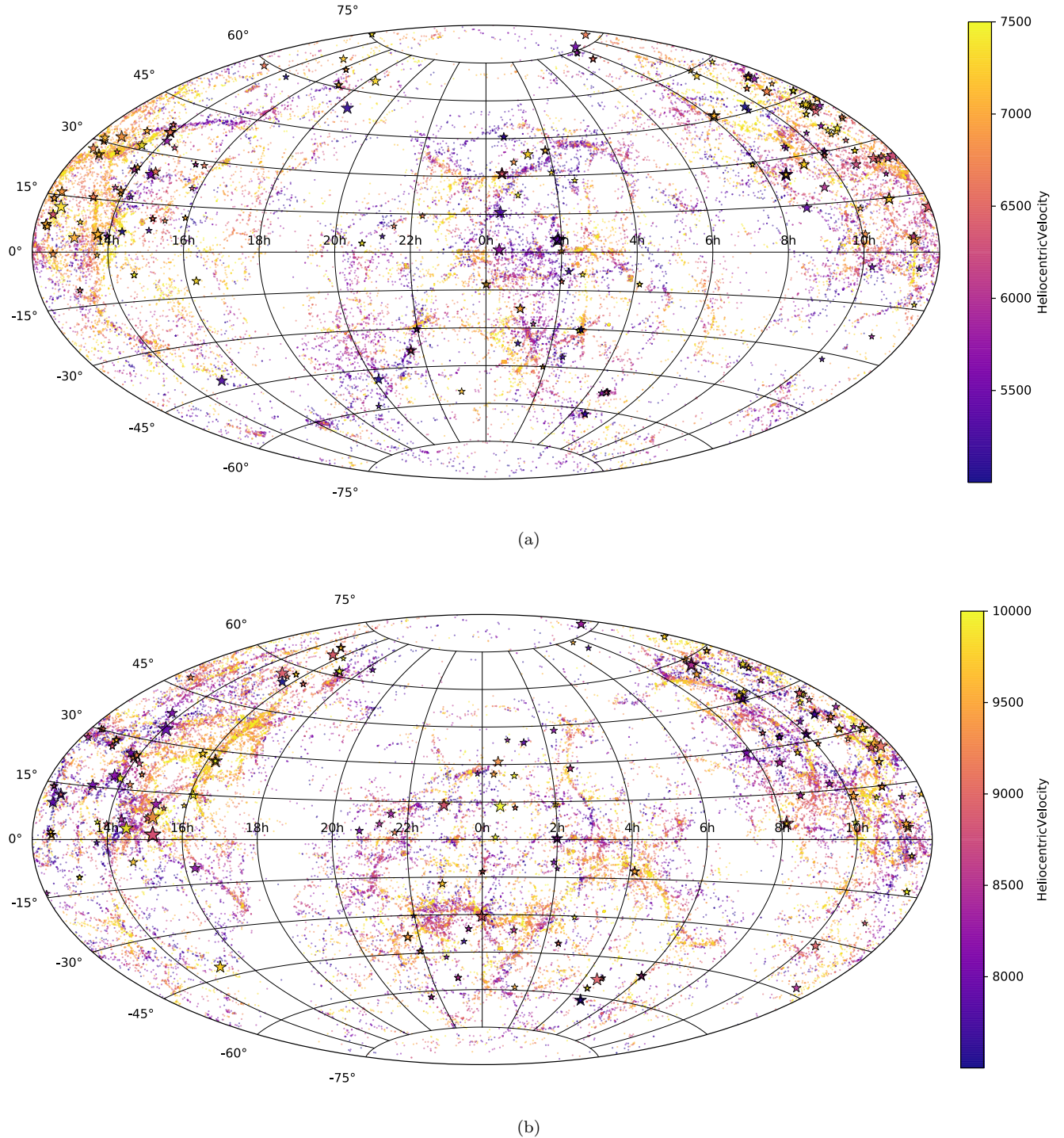


Figure 2. All sky maps of the locations of all absorbers and galaxies. Absorbers are plotted as stars and scaled in size based on their EW. Galaxies are plotted as dots. The colors of both galaxies and absorbers are mapped to their heliocentric velocities. (a) All galaxies and absorbers in the velocity range $5000 < cz \leq 7500 \text{ km s}^{-1}$. (b) All galaxies and absorbers in the velocity range $7500 < cz \leq 10,000 \text{ km s}^{-1}$.

Table 2. Summary of \mathcal{L} Variants

\mathcal{L} Variant	$\mathcal{L} - \text{isolated}$	$\mathcal{L} - \text{associated-isolated}$	$\mathcal{L} - \text{associated}$	$\mathcal{L} - \text{two+}$
Total number of Ly α absorbers: 1135 571 are <i>isolated</i> regardless of normalization				
$\mathcal{L}_{\min} = 0.01, rigor = 5$ (<i>Standard</i>)	267	56	146	58
$\mathcal{L}_{\min} = 0.01, rigor = 5, A = 2 \text{ if } \rho \leq R_{\text{vir}}$	267	56	160	55
$\mathcal{L}_{\min} = 0.001, rigor = 5$	227	69	167	65
$\mathcal{L}_{\min} = 0.001, rigor = 6$	227	69	162	68
$\mathcal{L}_{\min} = 0.001, rigor = 7$	227	69	154	75
$\mathcal{L}_{\min} = 0.001, rigor = 8$	227	69	145	78
$D^{1.5}, \mathcal{L}_{\min} = 0.001, rigor = 5$	317	39	174	32
$\mathcal{L}_{\min} = 0.001, rigor = 5, A = 2 \text{ if } \rho \leq R_{\text{vir}}$	227	69	181	62
$\mathcal{L}_{\min} = 0.005, v_{\text{norm}} = 150, rigor = 5$	265	58	148	63
$\mathcal{L}_{\min} = 0.005, v_{\text{norm}} = 250, rigor = 5$	246	64	151	64

NOTE—A summary of the subset sizes resulting from varying the likelihood metric’s normalization parameters. Different choices of normalization are simply shifting some of the non-*isolated* absorbers between different bins.

2.1. Sub-sample selection

A major hurdle for galaxy-absorber correlation studies has always been matching any particular absorption line to a single nearby galaxy. The basic premise of matching relies on the assumption that, in at least some cases, one particular galaxy’s potential, angular momentum, and radiation field dominates what an absorber “feels” (i.e., is the primary influencer for the EW, column density and Doppler b -parameter of an absorber). With this assumption in place, the issue becomes that galaxies are generally not isolated. When faced with a distribution of galaxies of differing types, sizes, orientations and distances (impact parameters) and velocities ($\Delta v = v_{\text{absorber}} - v_{\text{galaxy}}$) from an absorption line, which, if any, are most likely to be “associated” with the line?

As first introduced in French & Wakker (2017), we employ a unique likelihood method for objectively matching absorbers with nearby galaxies in a consistent, analytical manner. We define likelihood, \mathcal{L} , as follows:

$$\mathcal{L} = A \times e^{-(\frac{\rho}{R_{\text{eff}}})^2} \times e^{-(\frac{\Delta v}{v_{\text{norm}}})^2}, \quad (1)$$

where A is a normalization constant, ρ is the impact parameter between a galaxy and sightline, R_{eff} is one of two possible “effective - radii” we use for galaxies (virial radius and $D^{1.5}$, or diameter to the 1.5 power), Δv is the velocity separation between absorber and galaxy heliocentric, and v_{norm} is a velocity normalization (equal to one of 150, 200, or 250).

We calculate \mathcal{L} for every absorber-galaxy combination, which then gives us a single number as a three-dimensional proxy for the physical separation between the two. Based on this \mathcal{L} we then separate our sample into the following 5 distinct bins: *isolated*, \mathcal{L} -*isolated*, \mathcal{L} -*associated-isolated*, \mathcal{L} -*associated*, and \mathcal{L} -*two+*. The *isolated* sample contains all the Ly α lines that are farther than 500 kpc and 400 km s $^{-1}$ from *any* galaxy.

The \mathcal{L} -*isolated* sample contains those Ly α lines are far enough away from any galaxy so as to not meet our minimum- \mathcal{L} criteria. The \mathcal{L} -*associated-isolated* sample contains those Ly α lines which meet our \mathcal{L} criteria to be associated with a single galaxy, and that galaxy is isolated by 500 kpc and 400 km s $^{-1}$. The \mathcal{L} -*associated* sample contains those Ly α lines which meet our \mathcal{L} criteria to be associated with a single galaxy, but that galaxy is *not* isolated. And finally, the \mathcal{L} -*two+* sample contains those Ly α lines which meet our minimum- \mathcal{L} criteria to be associated with *more* than one galaxy.

Our standard criteria for a positive galaxy-absorber association are $\mathcal{L} \geq 0.01$ and $\mathcal{L}_1 \geq rigor \times \mathcal{L}_2$ with *rigor* = 5 (i.e., the \mathcal{L} -value for the most likely associated galaxy must be at least 5 times greater than that for the second most likely galaxy). However, we have also explored the results of adjusting the several possible \mathcal{L} normalizations. We calculate \mathcal{L} with R_{eff} equal to R_{vir} and $D^{1.5}$ and v_{norm} equal to 150, 200, and 250. For each of these combinations, we also calculate a variant with $A = 1$ and another with $A = 2$ if $R_{\text{eff}} \geq \rho$, and $A = 1$ otherwise. Additionally, we investigate the effect of changing the minimum- \mathcal{L} criteria to 0.005 and 0.001, and *rigor* = 5, 6, 7, and 8. Table 2 summarizes the resulting subsets for each of these combinations.

Overall, we find that none of these adjustments have a major effect on the resulting samples. To check, we performed Anderson-Darling statistical distribution analyses to check for differences between the EW distributions for each \mathcal{L} -variant and found no statistically significant difference between matching subsets (e.g., the EW distribution for the \mathcal{L} -*associated* subset does not change significantly between these different \mathcal{L} variants). For the remainder of this analysis we will concentrate on the $\mathcal{L}_{\min} = 0.01, v_{\text{norm}} = 20, A = 2$ normalization subsets. This matches the normalization we adopted in French & Wakker (2017), and represents a middle

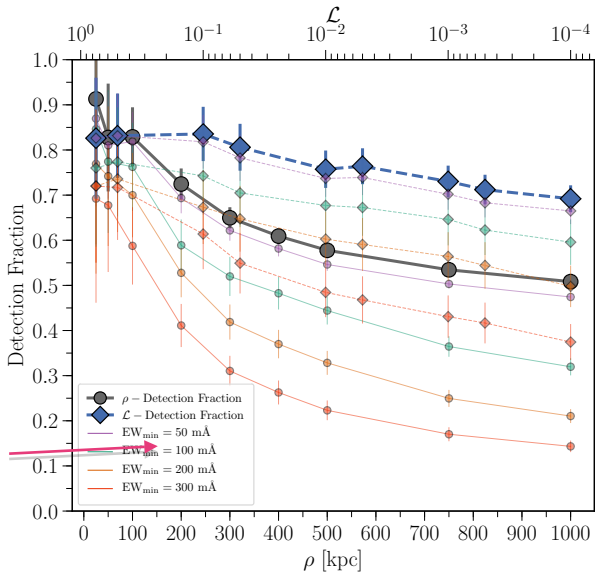


Figure 3. The detection fraction as a function of impact parameter (grey-circles) and \mathcal{L} (blue-diamonds). Note that the impact parameter and \mathcal{L} x -axis scales are quite different; the lowest \mathcal{L} bin (0.0001) corresponds to $\sim 3R_{\text{vir}}$, whereas the largest impact parameter bin (1000 kpc) is generally $\gg 3R_{\text{vir}}$. Error bars show the 1σ Poisson errors.

ground option while also maximizing the size of the $\mathcal{L}-\text{isolated-associated}$, $\mathcal{L}-\text{associated}$, and $\mathcal{L}-\text{two+}$ subsets.

3. RESULTS & DISCUSSION

3.1. Detection Fraction

First we explore the Ly α detection fraction as a function of galaxy proximity. To calculate this, we start by correlating the position of every QSO with our galaxy sample. For every galaxy found within 1000 kpc in physical impact parameter of each sightline we then check if a Ly α line appears in that sightline and within 400 km s^{-1} of the galaxy's systemic velocity. This results in a detection fraction as a function of impact parameter. Additionally, we calculate the detection fraction as a function of likelihood, \mathcal{L} , in a similar manner. However, as we are calculating detection fraction without any a priori knowledge of the velocity of the absorption lines, the likelihood function we use is modified from Eq. 1 to simply $e^{-(\rho/R_{\text{vir}})^2}$, or only the impact parameter - virial radius portion of our usual likelihood function given by Eq. 1. Note that this adjusted likelihood function is identical to Eq. 1 when $\Delta v = 0$.

We have plotted the detection fraction as a function of both impact parameter and \mathcal{L} in Figure 3. We also display the detection fraction for minimum Ly α EWs of 50, 100, 200, and 300 m \AA in purple, green, orange, and red (respectively). As expected, the detection fraction clearly increases with decreasing impact parameter and

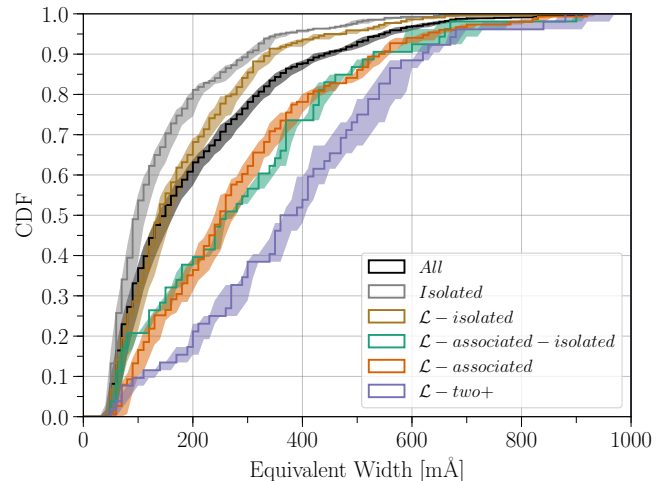


Figure 4. The equivalent width (EW) cumulative distribution function for each subset of our Ly α absorber sample. From the top-left corner to the bottom-right the curves are the fully isolated absorbers (grey), the absorbers isolated enough from any galaxy to not be likelihood-matched (brown), the full distribution (black), the absorbers likelihood-matched to a single, non-isolated galaxy (orange), the absorbers matched to a single, isolated galaxy (green), and the absorbers likelihood-matched with two or more galaxies (purple). The shaded region around each curve gives the EW measurement errors. Only $\text{EW} \geq 50 \text{ m}\text{\AA}$ absorbers are included to mitigate any bias due to the detection limit of lower-SN targets.

increasing \mathcal{L} . However, while the detection fraction continues to rise all the way to the 25 kpc mark however, it levels off at $\sim 1.5R_{\text{vir}}$ ($\sim 0.1\mathcal{L}$) as a function of likelihood. **WHY? MORE**. While the detection fraction does not fall below $\sim 50\%$ when including all absorbers, it falls off more quickly for stronger absorbers (e.g., to below $\sim 20\%$ for $\text{EW} \geq 300 \text{ m}\text{\AA}$ absorbers). **MORE**

3.2. Equivalent Width

Here we explore the effect of environment on the equivalent width of our Ly α absorber sample. Figure 4 shows the cumulative distribution function of equivalent widths for each of our 5 likelihood-separated subsets, along with that of the entire sample in black). We have only included $\text{EW} \geq 50 \text{ m}\text{\AA}$ here to mitigate any bias due to the detection limit of lower-SN targets. We find that each subset occupies a distinct space aside from the $\mathcal{L}-\text{associated-isolated}$ and $\mathcal{L}-\text{associated}$ sets, which are essentially indistinguishable. The physical result of this is that the strength EW of Ly α absorption depends strongly on environment. Stronger absorption lines are preferentially found near to galaxies, and the strongest lines are found near multiple galaxy systems. The result of Anderson-Darling sta

Clearly this is because the galaxies are embedded in filaments that contain gas (Wakker + 2015), so far from the galaxy it is no longer the galaxy, but the general environment

Need bigger contrast between types.

Brighter colors or bigger symbols

or more different symbols.

Or four plot panels.

Alos could separate into bins of delta v.

Absorbers closer in v could be closer to galaxy?

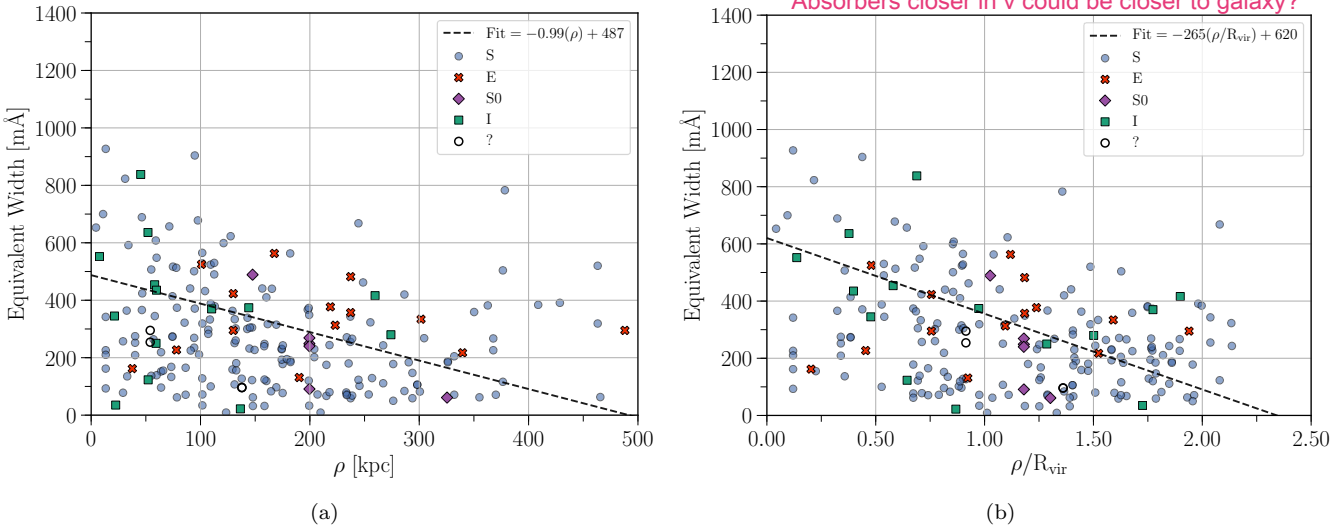


Figure 5. Left: The equivalent width (EW) of absorbers a function of impact parameter (ρ) to the associated galaxy. The best fit shown by the dashed-black line has the form: $EW = m(\rho) + b$, with $m = -0.99 \pm 0.25$ and $b = 487 \pm 49$. **Right:** The EW of absorbers a function of impact parameter to the associated galaxy normalized by the galaxy virial radius (ρ/R_{vir}). The best fit shown by the dashed-black line has the form: $EW = m(\rho/R_{\text{vir}}) + b$, with $m = -265 \pm 48$ and $b = 620 \pm 59$. **Both:** All \mathcal{L} – *associated – isolated* and \mathcal{L} – *associated* systems are included here. Blue-circles indicate spiral-type galaxies, green-squares indicate irregulars, red-crosses indicate ellipticals, purple-diamonds indicate S0's, and open black-circles indicate ambiguous morphological types.

stistical distribution tests between each subset indicate that our *isolated* and \mathcal{L} – *isolated* subsets are distinct from each of \mathcal{L} – *two+*, and \mathcal{L} – *associated – isolated* and \mathcal{L} – *associated* at a $> 95\%$ confidence level. Because \mathcal{L} – *associated – isolated* and \mathcal{L} – *associated* are found to be nearly indistinguishable via these test and by-eye, we will combine them for the remainder of this analysis.

This separation between EW distributions based on galaxy proximity is likely an effect of the distribution of the cosmic web; multiple galaxies should form from denser sections and intersections of intergalactic filaments, and these environments should thus also produce a stronger absorption profile.

This result on its own does not however illuminate any deeper connection or relationship between the individual galaxies and absorbers. Let us now consider the dependence of EW on galaxy impact parameter, as illustrated in Figure 5(a). We have also plotted EW as a function of virial radius normalized impact parameter (ρ/R_{vir}) in Figure 5(b). Firstly, we notice that weak ($EW \lesssim 400$ mÅ) absorbers are found at all impact parameters and ρ/R_{vir} , which agrees with our findings above from Figure 4. Moreover, absorbers stronger than $EW \sim 400$ mÅ are preferentially found close to galaxies, and absorbers with $EW \sim 800$ mÅ are *only* found within 100 kpc and $1R_{\text{vir}}$. Hence, weak $EW \lesssim 400$ mÅ absorbers are most likely Ly α -forest material, while the stronger absorbers are associated with the galaxies.

Secondly, we have included linear fits in both Figures 5(a) and 5(b) as shown by the dashed-black lines. In

each case we find a strong negative slope, and by eye the virial radius normalized version appearing to be the stronger correlation. To test this we calculated the Pearson correlation coefficient r -value for each fit. For the purely impact parameter correlation we find a Pearson r -value = -0.26 , with a p -value of $p = 1.2 \times 10^{-4}$, which indicates a weak but statistically significant negative correlation. For the virial radius normalized correlation we find $r = -0.35$ with $p = 1.2 \times 10^{-7}$, indicating a stronger and *more significant* negative correlation. If true, then the EW of Ly α absorption depends on the size of galaxy halos. Hence, either the physical or number density (or both) of absorbing cloudlets is greater closer to galaxies in a halo-scale dependent manner. The increased density of this neutral material could signify both inflows or outflows from galaxies, with inflows expected to harbor a greater fraction of the cool, neutral H I most readily traced by Ly α . An analysis of metals associated with these neutral cloudlets could provide clues to which is the mechanism source at play here.

Thirdly, let us consider the affect of galaxy morphology on the associated absorption, which we have indicated in Figure 5 by the color and style of the plot points. In each figure blue-circles indicate spiral-type galaxies, green-squares indicate irregulars, red-crosses indicate ellipticals, purple-diamonds indicate S0's, and open black-circles indicate ambiguous or unknown types. Spiral galaxies are clearly the dominant type, and are found at all impact parameter and EW. **WHAT FRACTION OF ALL GALAXIES ARE SPIRAL VS E?** Ir-

regulars are the next most common, but are not spread around as evenly. All but two irregular-type systems are separated by less than 150 kpc in Figure 5(a), and few low-EW absorbers are found within $\sim 0.5R_{\text{vir}}$ in Figure 5(b). In the first case, this can be explained by irregulars having a smaller average size ($\bar{R}_{\text{vir}} = 101$ kpc for irregulars, compared to 145, 178, and 194 kpc for spirals, S0's, and ellipticals). When normalized by virial radius however, the lack of low-EW absorbers at low ρ/R_{vir} could be an indication of more gas-rich halos. This would make sense, since irregular galaxies are often tidally disturbed due to recent interactions which can result in extended, gas-rich halos.

Finally, we also see that elliptical and S0 galaxies are associated with mostly low-EW absorption, especially within 100 kpc and $\sim 0.5R_{\text{vir}}$. **MORE**

3.3. Doppler b -parameter

Here we explore the effect of environment on the Doppler b -parameter of our Ly α absorber sample. In an analogous fashion as above, Figure 6 shows the cumulative distribution functions for the Doppler b -parameters of each subset of absorbers. Similar to the EW result, the Doppler b -parameters trend toward larger values based on their proximity to galaxies. The separation here however is far weaker. While the separation between, e.g., *isolated* and \mathcal{L} – *two+* samples, remains statistically significant, we cannot claim any further significance between the other subsets. Because our b -parameters are derived via the second moment of the apparent optical depth profile, these b -parameter estimates become highly uncertain for $\text{EW} \gtrsim 350$ mÅ. For these stronger lines the profile becomes saturated, producing a degeneracy between EW and b . Unfortunately these are the very lines we expect to be most associated with near or multiple galaxy galaxy systems. A careful profile fitting analysis is the best way forward here, which we will reserve for a future work.

3.4. Inclination

Here we investigate the inclination dependence of Ly α absorber properties. In Figure 7 we display the distribution of all associated galaxies alongside the distribution of all galaxy inclinations in the survey volume (again, \mathcal{L} – *associated* – *isolated* and \mathcal{L} – *associated* subsets are combined here; see Chapter 1 for a full discussion of our galaxy dataset). As we first discovered in French & Wakker (2017), there is an overabundance of absorbers associated with high-inclination galaxies. To test the significance of this overabundance we used the Anderson-Darling statistical distribution test, which yields a p -value of $AD_p = 7.2 \times 10^{-6}$. For a normal distribution this corresponds to $\sim 4.5\sigma$, indicating with a high confidence limit that these associated galaxies are *not* drawn from the same distribution as the all-sky galaxy population.

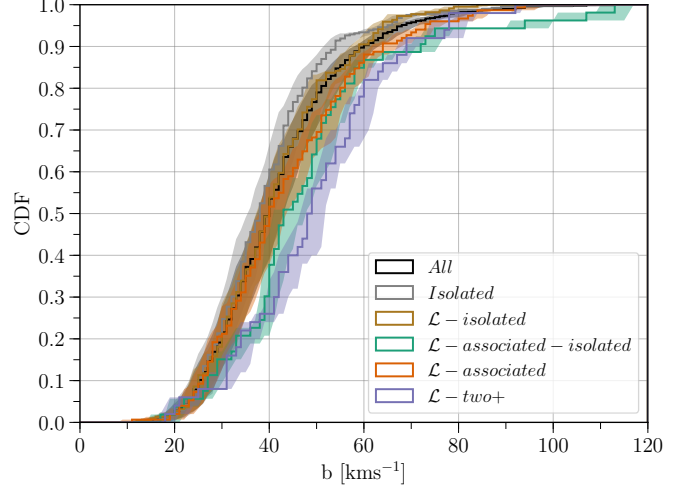


Figure 6. The Doppler b -parameter (b) cumulative distribution function for each subset of our Ly α absorber sample. From the top-left corner to the bottom-right the curves are the fully isolated absorbers (grey), the absorbers isolated enough from any galaxy to not be likelihood-matched (brown), the full distribution (black), the absorbers likelihood-matched to a single, non-isolated galaxy (orange), the absorbers matched to a single, isolated galaxy (green), and the absorbers likelihood-matched with two or more galaxies (purple). The shaded region around each curve gives the b -parameter measurement errors. Only $\text{EW} \geq 50$ mÅ absorbers are included to mitigate any bias due to the detection limit of lower-SN targets.

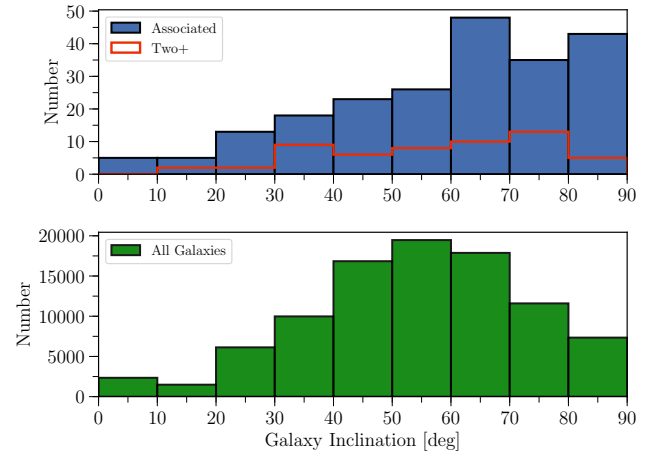


Figure 7. Top: The distribution of all associated galaxy inclinations is shown in blue. The overlaid red histogram shows the distribution of the highest \mathcal{L} -galaxy inclinations from the \mathcal{L} – *two+* subset. **Bottom:** The distribution of all galaxies in the survey volume (i.e., $cz \leq 10,000$ km s $^{-1}$).

To further explore this phenomenon we have also calculated the detection fraction as a function of inclination

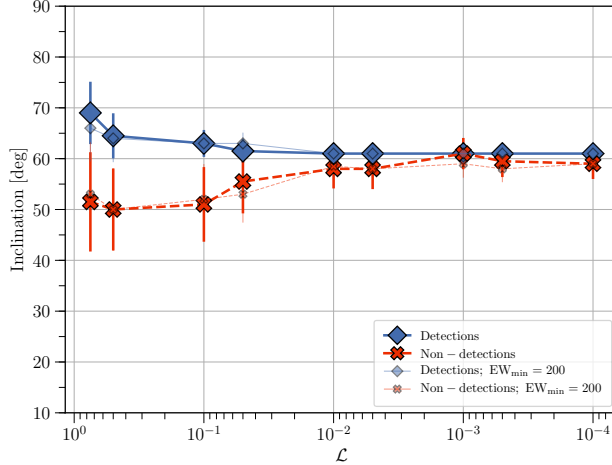


Figure 8. The median inclination of galaxies is shown as a function of likelihood \mathcal{L} for both detection (blue-diamonds) and non-detections (red-crosses) of associated absorbers. Detection and non-detection median inclinations are also shown for $\text{EW} = 200 \text{ m}\text{\AA}$ minimum absorber equivalent widths by the thinner, semi-transparent lines.

and likelihood \mathcal{L} . Figure 8 shows the median inclination as a function of \mathcal{L} for galaxies. For a galaxy at a given value of \mathcal{L} , the solid blue-diamond line gives the median inclination if we detect an absorber within $\Delta v \leq 400 \text{ km s}^{-1}$, and the dashed blue-cross line gives the same for systems *without* a Ly α detection. The error bars shown are calculated by a 10,000 repetition bootstrap analysis with replacement (i.e., we randomly resample the distribution of inclinations while allowing for duplicate entries, and then compute the standard deviation of the resulting sample distribution). Figure 8 shows that at very low \mathcal{L} both detections and non-detections have the same median inclination, but the distributions then split at higher \mathcal{L} where the sightline is closer to the galaxy halos. Thus, we are more likely to detect an absorber near a highly inclined galaxy.

This result is most easily explained by evoking a non-spherical H I galaxy halo. For example, if absorbers are distributed in a perfectly spherical manner around galaxies, then we would expect just as many non-detections as detections at any given galaxy inclination and impact parameter (or likelihood) from a sightline. We do not find this. Thus, the distribution of Ly α absorbers around galaxies must be non-spherical, with a flattened, disk-like Ly α halo fitting the bill nicely.

3.5. Azimuth

Here we investigate the dependence of Ly α absorber properties on their orientation with respect to the major axis of nearby galaxies. Figure 9 shows the distribution of azimuth angles for systems from the combined $\mathcal{L} - \text{associated}$ and $\mathcal{L} - \text{associated} - \text{isolated}$ subsets in blue, along with the distribution for the $\mathcal{L} - \text{two+}$ sub-

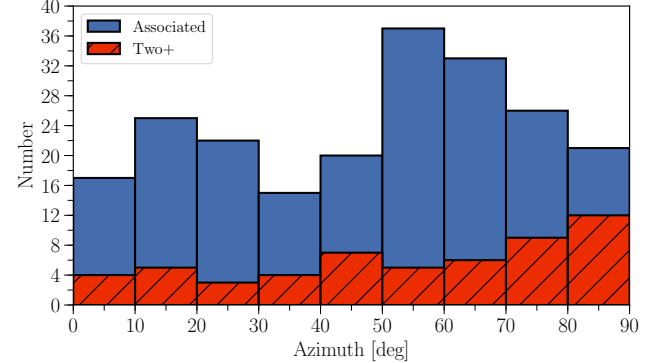


Figure 9. The distribution of azimuth angles for the combined $\mathcal{L} - \text{associated}$ and $\mathcal{L} - \text{associated} - \text{isolated}$ subsets is shown in blue, with the $\mathcal{L} - \text{two+}$ subset shown in red.

set in red. There appears to be a bimodal distribution here, with an excess of absorbers near low (major-axis) and high (minor-axis) azimuth angles. The same is not seen for the $\mathcal{L} - \text{two+}$ subset, suggesting the presence of other nearby galaxies may be stirring up the Ly α absorbing material in these galaxies' halos. It is commonly expected that gas found near the major axis of a galaxy represents accreting material, while material around the minor axis represents outflows CITE??.

MORE

4. SUMMARY

1. Ly α absorbers with $\text{EW} \lesssim 100 \text{ m}\text{\AA}$ are ubiquitous, making up nearly 50% of all Ly α systems in the nearby Universe, and do not correlate strongly with environment (70% of these weak absorbers are isolated).

2.

5. FUTURE WORK

We have established large, rich dataset with which to explore the relationship between circumgalactic material and the galaxies that reside in it. Much can still be learned by continuing to delve deeper into this data. The first future goal we have is to produce galaxy-Ly α two-point cross-correlation functions, as has been demonstrated by, e.g., Chen et al. (2005), among others. This will be our first goal as it does not involve any significant additions to the data already presented here.

Our next goal will be to produce Voigt profile fits for each absorber. While equivalent widths and second-moment derived b -parameters are an incredibly convenient and powerful tool to study

Metals

This research has made use of the NASA/IPAC Extragalactic Database (NED) which is operated by the Jet Propulsion Laboratory, California Institute of Technology, under contract with the National Aeronautics and Space Administration. Based on observations with

the NASA/ESA *Hubble Space Telescope*, obtained at the Space Telescope Science Institute (STScI), which is operated by the Association of Universities for Research in Astronomy, Inc., under NASA contract NAS 5-26555. Spectra were retrieved from the Barbara A. Mikulski Archive for Space Telescopes (MAST) at STScI. Over the course of this study, D.M.F. and B.P.W. were supported by grant XXXX

Facility: HST (COS)

REFERENCES

- Bowen, D. V., Pettini, M., & Blades, J. C. 2002, ApJ, 580, 169
- Bowen, D. V., Pettini, M., & Boyle, B. J. 1998, MNRAS, 297, 239
- Chen, D. N., Jing, Y. P., & Yoshikawa, K. 2003, ApJ, 597, 35
- Chen, H.-W., Prochaska, J. X., Weiner, B. J., Mulchaey, J. S., & Williger, G. M. 2005, ApJL, 629, L25
- Chen, H.-W., & Tinker, J. L. 2008, ApJ, 687, 745
- French, D. M., & Wakker, B. P. 2017, ApJ, 837, 138
- Lanzetta, K. M., Bowen, D. V., Tytler, D., & Webb, J. K. 1995, ApJ, 442, 538
- Steidel, C. C., Erb, D. K., Shapley, A. E., et al. 2010, ApJ, 717, 289
- Wakker, B. P., & Savage, B. D. 2009, ApJS, 182, 378